Published online 8 September 2006 *Nucleic Acids Research, 2006, Vol. 34, No. 16* ***4593–4608***
doi:10.1093/nar/gkl603

NOP132 is required for proper nucleolus localization of DEAD-box RNA helicase DDX47

Takeshi Sekiguchi*, Toshiya Hayano[1], Mitsuaki Yanagida[1], Nobuhiro Takahashi[1] and Takeharu Nishimoto

Department of Molecular Biology, Graduate School of Medical Science, Kyushu University, 3-1-1 Maidashi, Higashi-ku, Fukuoka 812-8582, Japan and [1]Department of Applied Biological Science, Tokyo University of Agriculture and Technology, 3-5-8 Saiwai-cho, fuchu, Tokyo 183-8509, Japan

Received April 5, 2006; Revised July 11, 2006; Accepted August 3, 2006

ABSTRACT

Previously, we described a novel nucleolar protein, NOP132, which interacts with the small GTP binding protein RRAG A. To elucidate the function of NOP132 in the nucleolus, we identified proteins that interact with NOP132 using mass spectrometric methods. NOP132 associated mainly with proteins involved in ribosome biogenesis and RNA metabolism, including the DEAD-box RNA helicase protein, DDX47, whose yeast homolog is Rrp3, which has roles in pre-rRNA processing. Immunoprecipitation of FLAG-tagged DDX47 co-precipitated rRNA precursors, as well as a number of proteins that are probably involved in ribosome biogenesis, implying that DDX47 plays a role in pre-rRNA processing. Introduction of NOP132 small interfering RNAs induced a ring-like localization of DDX47 in the nucleolus, suggesting that NOP132 is required for the appropriate localization of DDX47 within the nucleolus. We propose that NOP132 functions in the recruitment of pre-rRNA processing proteins, including DDX47, to the region where rRNA is transcribed within the nucleolus.

INTRODUCTION

Ribosome biogenesis is a highly complex and coordinated process that occurs not only in the nucleolus but also in the nucleoplasm and cytoplasm (1) that has been studied extensively in yeast systems using both biochemical and genetic analyses (2). Based on the protein composition of several yeast ribosomal subunit precursors recently characterized by proteomic approaches, more than 170 factors are predicted to participate in ribosome biogenesis [see review in (3)]. Thus, proteomic approaches have provided additional evidence for a ribosome assembly pathway in eukaryotes and have confirmed the dynamics of the entire process (4).

Ran is a member of the Ras superfamily of small G proteins and a nuclear protein with several functions, including nucleocytoplasmic transport of many types of proteins and of nucleic acids across nuclear membranes and ribosome biogenesis through Dis3, an exosome subunit (5–9). The gene encoding the yeast homolog of RCC1 (*SRM1*), the guanine nucleotide exchange factor for Ran, genetically interacts with *GTR1* in yeast (10). Gtr1 and Gtr2 are associated with each other and belong to a novel subfamily of small G proteins (11) and play various roles in cellular metabolism (12,13). Gtr1 is associated with Rpc19 (14) and Nop8 (15) which is an essential nucleolar protein required for 60S ribosome biogenesis (16) and is associated with nucleolar protein Nip7 (17), suggesting that Gtr1 could play roles in multiple steps of ribosome biogenesis. Human RRAG A/Rag A/FIP-1 is a functional homolog of yeast Gtr1 (18) and is associated with an essential nucleolar protein, NOP132, which interacts with RRAG C, RRAG D, and human NIP7 and might anchor these proteins to the nucleolus (15). Amino acid sequence comparison revealed that NOP132 is similar to yeast Nop8. Thus, NOP132 might have a role in ribosome biogenesis. NOP132 was found to be upregulated in diffuse-type gastric cancer in an attempt to identify novel therapeutic targets for this disease (19).

RNA helicases from the DEAD-box family are present in almost all organisms and have important roles in RNA metabolism. They participate in many processes, such as the synthesis, processing, export, and degradation of RNA [see review in (20)]. In humans, 36 members of the DEAD-box family of putative RNA helicases have been identified and are hypothesized to have roles in differentiation and carcinogenesis (21). *Saccharomyces cerevisiae* has

*To whom correspondence should be addressed. Tel: +81 92 642 6177; Fax: +81 92 642 6183; Email: sekigu@molbiol.med.kyushu-u.ac.jp
Present addresses:
Toshiya Hayano, Department of Bioscience and Bioinformatics, College of Information Science and Engineering, Ritsumeikan University, 1-1-1 Nojihigashi, Kusatsu 525-8577, Japan
Mitsuaki Yanagida, Institute for Environmental and Gender Specific Medicine, Juntendo University, Graduate School of Medicine, 2-1-1, Tomioka, Urayasu, Chiba 279-0021, Japan

26 DEAD-box proteins, many of which are involved in ribosome biogenesis (20).

Here we used a proteomic approach to elucidate the function of NOP132 in human cells. We identified NOP132-associated proteins by mass spectrometric analysis; among the identified proteins were the nucleolar DEAD-box RNA helicases DDX47 and DDX18. We also showed that DDX47-associated proteins are very similar to those associated with NOP132. Because FLAG-tagged DDX47 could be co-precipitated with rRNA precursors, DDX47 may be involved in pre-rRNA processing. To understand the significance of the association of NOP132 with DDX47, we examined the subcellular localization of DDX47 upon downregulation of NOP132 by RNA interference (RNAi). NOP132 downregulation caused mislocalization of DDX47. Herein we propose that NOP132 recruits DDX47 protein to the center of the nucleolus, where it functions in the processing of primary rRNA transcripts.

MATERIALS AND METHODS

Cell culture and transient transfection

BHK21, 293, 293EBNA, and HeLa cells were grown at 37.5°C in Dulbecco's modified Eagle medium containing 10% fetal calf serum, penicillin (100 U/ml), and streptomycin (100 μg/ml) in an incubator under 10% CO_2 or, for 293EBNA cells, 5% CO_2. Cells were washed with TD buffer (25 mM Tris-HCl, pH 7.4; 136.8 mM NaCl; 5 mM KCl; and 0.7 mM Na_2HPO_4). BHK21 and 293 cells (1×10^5 cells) were transfected with 1 μg vector and 7 μl LipofectAMINE™ Reagent (Life Technologies, Rockville, MD) per 35 mm dish for immunofluorescence experiments. For FLAG-tagged protein co-precipitation experiments, 293EBNA and 293 cells (5×10^5 cells) were transfected with 5 μg vector and 30 μl LipofectAMINE™ Reagent per 100 mm dish for 4 h in the absence of serum and antibiotics, as recommended by the supplier, and then cells were incubated at 37.5°C as previously described (22).

Immunoprecipitation and protein identification by peptide mass fingerprinting

At 48 h post-transfection, 293EBNA cells were harvested and washed with phosphate-buffered saline (PBS) and lysed on ice for 30 min in lysis buffer (50 mM Tris–HCl, pH 8.0; 150 mM NaCl; and 0.5% (w/v) IGEPAL CA630) containing a protease inhibitor mixture. One sample (Figure 1, lane 3) was sonicated on ice for 1 s (Sonicator™; Heat System-Ultrasonics Inc., Farmingdale, NY), with a microtip, 40% cycle, and output control of 4. The soluble fraction was obtained by centrifugation at 15 000 rpm for 30 min at 4°C and incubated with 20 μl anti-FLAG M2-agarose beads (Sigma-Aldrich, St Louis, MO) for 4 h at 4°C to immunoprecipitate NOP132-associated complexes. After the beads were washed five times with lysis buffer and once with 50 mM Tris–HCl, pH 8.0/150 mM NaCl, complexes bound to the agarose beads were eluted with 20 μl 50 mM Tris–HCl, pH 8.0/150 mM NaCl containing 500 μg/ml FLAG peptide. The eluted complexes were analyzed by SDS–PAGE. Protein-containing SDS–PAGE gel fragments were subjected to in-gel digestion with trypsin as previously described (23). The resulting peptides were recovered and analyzed for peptide mass fingerprinting using a PE Biosystems Voyager DE-STR (Perkin-Elmer, Inc., Wellesley, MA) as described previously (23). Peptide masses were searched with 50 p.p.m. mass accuracy using the database fitting program MS-Fit (available at prospector.ucsf.edu), and protein identification was performed according to the criteria described previously (23). When identification was unsuccessful using this method, the digested sample was analyzed by the LC-MS/MS method described below.

Protein Identification by LC-MS/MS Analysis

NOP132-associated complexes were digested with endoproteinase Lys-C, and the resulting peptides were analyzed using a nanoscale LC-MS/MS system as described (24). The peptide mixture was applied to a Mightysil-RP-18 (3 μm particle; Kanto Chemical, Osaka, Japan) fritless column (45 mm × 0.150 mm, i.d.) and separated using a 0–40% acetonitrile gradient containing 0.1% formic acid over 80 min at a flow rate of 50 or 25 nl/min. Eluted peptides were sprayed directly into a quadrupole time-of-flight hybrid mass spectrometer (Q-ToF 2; Micromass, Wythenshawe, UK). MS/MS spectra were acquired by data-dependent collision-induced dissociation, and MS/MS data were analyzed using MASCOT software (Matrix Science, London, UK) for peptide assignment. The criteria were in accordance with the manufacturer's instructions. If necessary, match acceptance of automated batch processes was confirmed by manual inspection of each set of raw MS/MS spectra in which the major product ions were matched with theoretically predicted product ions from the database-matched peptides. A mock eluate, which used anti-FLAG with the FLAG peptide, was analyzed by the same LC-MS/MS method as used for the NOP132-associated complexes and the identified proteins were then subtracted from the proteins identified in the FLAG-NOP132 co-precipitations. Thus, those proteins identified in the mock eluate were not included in the list of NOP132-associated proteins unless a quantitative increase was confirmed.

Purification of GST-fusion proteins

An *Escherichia coli* BL21 strain carrying a GST plasmid was grown in 750 ml of Luria–Bertani medium and was treated with isopropyl β-D-thiogalactoside (final conc., 0.2 mM) for 4 h at 30°C as previously described (8). Cells were dispersed in lysis solution (1× PBS, 2 mM EDTA, 0.1% β-mercaptoethanol, 0.2 mM phenylmethyl sulfonyl fluoride, and 10 μg/ml aprotinin) at a ratio of 1:5 (cell volume: lysis solution) and were sonicated on ice three times for 5 min each, with a microtip, 40% cycle, and output control of 4. After two rounds of centrifugation at 10 000 *g* for 10 min at 4°C, 10 ml of the supernatant was mixed with 1 ml of a 50% (v/v) slurry of glutathione-Sepharose-4B beads (GE-Healthcare) and rotated for 30 min at 4°C. The beads were washed four times with the lysis buffer.

In vitro binding assay

For the *in vitro* binding assay, a Sf9 cell lysate expressing baculovirus-produced NOP132 was obtained by infecting

Sf9 cells with recombinant baculoviruses encoding NOP132 as described previously (15). Briefly, Sf9 cells were cultured in 250 ml disposable Erlenmeyer flasks at 27°C under rotation at 125 r.p.m. in Grace's insect medium (Invitrogen) supplemented with 10% fetal calf serum, penicillin (100 U/ml), and streptomycin (100 μg/ml). Cells were maintained at a density of 0.5–6.0 × 10^6 cells/ml. Cells were seeded at 3.0 × 10^6 cells/ml and infected with a 1:100 dilution of baculovirus stocks, and cultured for 48–72 h. The cells were collected and lysed with the immunoprecipitation buffer [50 mM Tris–HCl, pH 7.4; 1 mM EDTA; 150 mM NaCl; 0.1% (v/v) Nonidet P40; 1 mM phenylmethyl sulfonyl fluoride; 0.1 μg/ml aprotinin; and 1 mM dithiothreitol (DTT)]. The extract was obtained by centrifugation at 13 000 *g* for 10 min at 4°C. The extract was diluted to 500 μl with immunoprecipitation buffer. Twenty microgram of either GST, GST-DDX47, GST-DDX18, or GST-GRWD1 bound to the glutathione-Sepharose-4B beads was mixed with baculovirus-produced NOP132. After incubation at 4°C for 30 min, the beads were pelleted, washed four times with immunoprecipitation buffer, and suspended in 50 μl of SDS–PAGE sample buffer (62.5 mM Tris–HCl, pH 6.8; 100 mM DTT; 2% (w/v) SDS; and 10% glycerol). Bound proteins were subjected to SDS–PAGE and NOP132 was detected using anti-NOP132N.

Immunoblotting and antibodies

Protein samples were subjected to SDS–PAGE using 5–20% gradient polyacrylamide gels (PAGEL, ATTO, Japan) and the protein bands were analyzed by immunoblotting. Immunopositive bands were visualized using the ECL kit (GE-Healthcare) as recommended by the supplier. The anti-NOP132N and anti-RRAG A antibodies were described previously (15). The anti-human DDX18 and DDX47 antibodies were raised by immunizing rabbits with GST-DDX18 and GST-DDX47 proteins, respectively, and were purified by affinity purification methods using GST-fusion proteins that were transferred onto a filter. Mouse anti-RAN (Cat. no. 610 340) was purchased from BD Bioscience (San Jose, CA).

Immunofluorescence

Transfected cells on coverslips were fixed with 1 ml 4% paraformaldehyde for 5 min and were processed for immunostaining as described (25). Cells were stained with 1 μg/ml Hoechst 33 342 and mounted with Vectashield or with Vectashield containing 4′-6-Diamidino-2-phenylindole (DAPI) (Vector Laboratories, Burlingame, CA). A Zeiss Axiophot microscope was used for sample analysis using standard microscopic methods. Digital imaging of the stained cells was also obtained using an Olympus laser-scanning microscope LSM-GB200 system, as described (18).

Yeast two-hybrid assay

A yeast two-hybrid assay (26) was performed using the *S.cerevisiae* Y190 strain (*a gal4 gal80 his3 trp1 ade2 ura3 leu2 URA3::GAL1-lacZ LYS2::GAL1-HIS3 cyh*^{r}) to test protein interactions *in vivo*, as described (22). *S.cerevisiae* cells were grown in YPD (2% glucose, 2% peptone, and 1% yeast extract) or SD-Trp-Leu-His + 3-Aminotriazol (2% glucose, 0.67% yeast nitrogen base without amino acids, and 25 mM 3-Aminotriazol, supplemented with all essential amino acids except for tryptophan, leucine, and histidine). Amino acids were added to a final concentration of 20–50 μg/ml. The solid media contained 2% agar in addition to the components described above. The β-galactosidase chromogenic filter assays were performed by transferring the yeast colonies onto nitrocellulose filters (Protran BA85; Schleicher and Schuell, Germany). The yeast cells were partially lysed by submerging the filters in liquid nitrogen for 1 min. Filters were processed as described previously (15). Color, representing a positive signal, appeared within 120 min at 30°C (Figure 7).

Recombinant DNA

Human DDX47 cDNA was isolated by RT–PCR using the human Burkitt's lymphoma cDNA library (Becton Dickinson, Franklin Lakes, NJ). DDX18 cDNA was purchased from Invitrogen (Carlsbad, CA). The control FLAG vector was pFLAG-CMV-5a (Sigma). Enhanced green fluorescent protein (EGFP)-NOP132 and the red fluorescent protein (DsRed)-NOP132 were used to visualize the subcellular localization of proteins as described (15). GST-DDX18, GST-DDX47, and GST-GRWD1 were constructed by inserting cDNA fragments into pGEX-KG. Deletion constructs of DDX47 and NOP132 in pAS1, pACT2, and pEGFPc1 vectors were prepared by PCR. Kiaa0539 cDNA was provided by Dr Ohara at the Kazusa DNA Research Institute (Chiba, Japan). The EcoRI–XhoI fragment of the Kiaa0539 cDNA was inserted into the EcoRI–XhoI sites of the pEGFPc2 vector. To obtain FLAG-Coil [without a nuclear localization signal (NLS)], a NOP132 cDNA fragment (nucleotide no. 2000–2870) was amplified by PCR and inserted into the EcoRI site of the pcDNA3.1 (Hygro) vector. Human ribosomal internal transcribed spacer 1 (ITS1), internal transcribed spacer 2 (ITS2), external transcribed spacer 2 (ETS2), 28S rRNA, 18S rRNA, and 5.8S rRNA were subcloned in the pUC118 vector. Each construct was checked by automated DNA sequencing using an ABI PRISM^R 3100 sequencer (Applied Biosystems, Foster City, CA).

RNAi

Two pairs of small interfering RNAs (siRNAs) were chemically synthesized (Hokkaido System Science, Sapporo, Japan) and annealed before transfection as described previously (27). Transfection was performed on 2 × 10^4 HeLa cells/20 mm tissue culture plate or 5 × 10^5 HeLa cells/90-mm tissue culture plate with a final concentration of 200 mM siRNA duplex using Oligofectamine reagent (Invitrogen) according to the manufacturer's instructions. Using fluorescein-isothiocyanate-conjugated control oligonucleotide, there was nearly 100% incorporation of the oligonucleotide under our experimental conditions, as observed under a fluorescence microscope. The oligonucleotide sequences used for NOP132 and DDX47 RNAi experiments were as follows: NOP132; mixtures of NOP132-B (5′-CACUUCACCUAAUGAGCCATT-3′/5′-UGGCUCAUU-AGGUGAAGUGTT-3′), and NOP132-C (5′-CAGUUUC-CUUAGGUGAGCCTT-3′/5′-GGCUCACCUAAGGAAAC-UGTT-3′) (15). DDX47; mixtures of DDX47-1

(5′-UGGAGUUAAGGGAGCAUGGAGTT-3′/5′-CUCCAUGCUCCCUUAACUCCATT-3′) and DDX47-2 (5′-GAUCCUCAAAGUGAUUCCUCGTT-3′/5′-CGAGGAAUCACUUUGAGGAUCTT-3′). Luciferase siRNA (28) was used as a control and was kindly provided by Dr H. Nishitani.

Isolation of nucleic acids and filter hybridization

The siRNA-treated HeLa cells were trypsinized and the cell number was determined using a Coulter counter (Beckman Coulter, Inc. Fullerton, CA). Total RNA was extracted using Trizol™ reagent as recommended by the supplier (Invitrogen). Total RNAs from about 4000 cells were electrophoresed in a 1.5% agarose-formaldehyde gel, transferred to a nylon Hybond-N membrane (GE-Healthcare) and cross-linked by UV irradiation. Northern blotting was performed as described previously (29). The DDX47-associated RNAs (Figure 4c) were isolated from FLAG-DDX47-transfected 293 cells and processed as described previously (30).

RESULTS

Identification of proteins in the NOP132 complex

In order to identify proteins that may interact with NOP132 in the cell, we used an anti-FLAG antibody to immunoprecipitate NOP132-associated proteins from human 293EBNA cells expressing FLAG-tagged NOP132. Anti-FLAG was used to

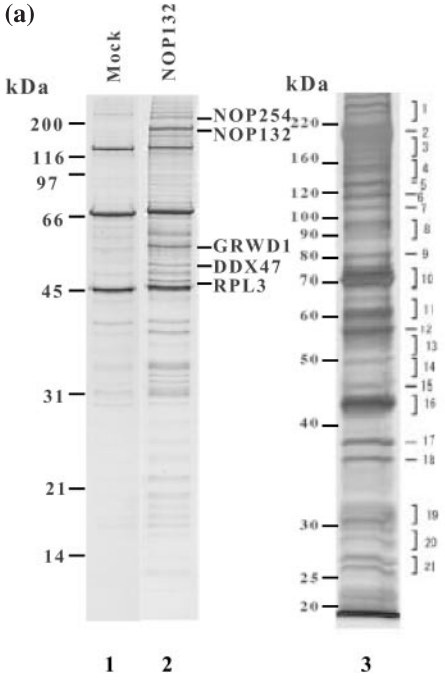

NOP132-associated proteins

bands	
1.	ASCC3L1,NOP254/C21orf108
2.	NOP132/NOL8
3.	SF3B1,KIAA0133
4.	RBM10,DHX9,SF3B3,TAF4,CLASP2.
5.	ANKFY1,HNRPU,JAK1,
6.	HSPA4,HSPH1,E2F7
7.	NCL,CDC5L,HSPA4L
8.	KPNB1,ILF3,HSPCA,DDX21,DHX15
9.	HSPA5,EIF4B,HSPA1L, HSPA6
10.	HSPA2, IVNS1ABP
11.	KPNA3, KPNA4, MAP3K7IP1,HSPD1,PRPF31, CCT6A
12.	GRWD1,LOC144097, TUBA6,VIM,PTBP1
13.	DDX47,TUBB,TUBB2A,TUBA1,TUBB4, HNRPH1, HNRPH2,*P53*, TUBB6
14.	RPL4, CSDA, HNRPF, EEF1G,EEF1A, WARS, DNAJA1, SSB, SF3B4, CDC37
15.	RPL3,PRL3L, HNRPD
16.	C14orf150,ACTS, RBMX,RPSA
17.	WDR57,NPM1,HNRPA1
18.	FBL, RPLP0,RPL6, HNRPA0
19.	RPS6,RPS3,RPS2,RPL8, RPS3A, HIST1H1C
20.	RPL7A,RPL7,RPS4, FHL2
21.	RPL10A,RPS8,RPL13,RPL14,RSMB

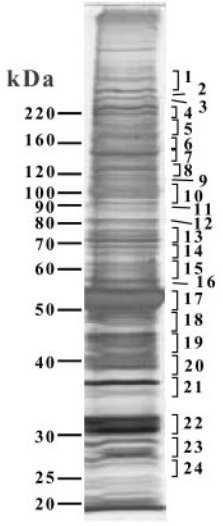

DDX47-associated proteins

bands	
1	FLNA
2	FAF-X, FAF-Y
3	NOP254/C21orf108
4	UBR2,PDCD11,HEATR1,BMS1L
5	LARP1,CTCF,BCLAF1,EIF3S10
6	SF3B1, MYBBP1A,KIAA0690
7	DHX9, C20orf6,FTSJ3,SART3,CEBPZ,RBM10,ZFR
8	FLJ10774,HNRPU,DDX24,FLJ12949,MATR3
9	NOL1, DDX10, MPHOSPH10, BOP1, GNL2, MOV10, C1orf107, C4orf9, XRN2, RBM28,
10	DDX21, NCL,KIAA0179, DDX27, NOC3L,NOC2L,AATF
11	DHX15, TBL3,DDX50,SDAD1
12	FLJ20758, NOL10, PABPC4, EIF4B, HP1BP3, PWP1
13	PABPC1,HNRPM,HSPA1L,NOL5A,HSPA6,HNRPR, HSPA9B, GTPBP4, WDR46, KIAA0020, CIRH1A, PES1
14	GNL3, RSL1D1, NOP5, IGF2BP1, IGF2BP3, SNRP70,IGF2BP2
15	HSPD1,CSDA,PRPF31,PPAN
16	GRWD1, KPNA2,
17	DDX47
18	RPL3, RPL4, HNRPF,LYAR,HRB2,RPL3L,YBX1
19	MRPS2,RPSA,RRS1,ILF2, EBNA1BP2,BXDC2,H2AFY2,PURA, HNRPAB
20	MRPS9, MRPS22, MRPS28, MRPS29, HNRPC, RARA,NPM1, H2AFY,SFRS10,HNRPCL1, HNRPA3
21	RPLP0, RPL10, RPL6, MK1671P, ABT1, HNRPA0, C14orf120, IGF2BP4,FBL
22	RPS3, RPS3A, LOC146053,RPL7A,RPS6,RPS2,RPL8,HIST1H1C
23	RPS4, RPL7L,WUGSC:H_RG054D04.1, H1FX, H1F0, SLC25A6
24	RPL10A, RPL7, RPS8,RPL13, SNRPB2,MRPS34,RPL7L1

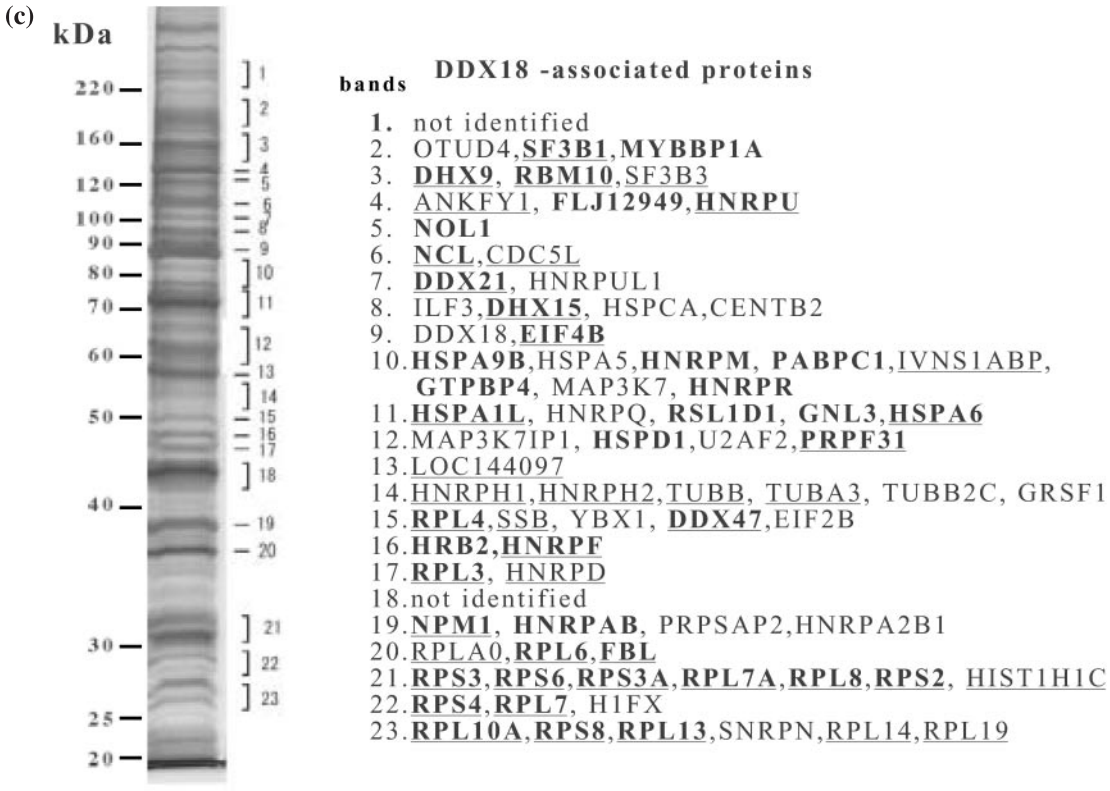

Figure 1. Protein components of immunoprecipitated FLAG-NOP132-, FLAG-DDX47-, and FLAG-DDX18-associated complexes. (**a**) Silver-stained SDS–PAGE gels of FLAG-NOP132-associated complexes immunoprecipitated with anti-FLAG from cells expressing FLAG-tagged NOP132. Lane 1, control immunoprecipitate (Mock) from untransfected 293EBNA cells; lane 2, 293EBNA cells expressing FLAG-tagged NOP132 (11% SDS–PAGE gel); lane 3, 293 cells expressing FLAG-tagged NOP132 (lysis by sonication, 10% SDS–PAGE gel)]. Molecular weight markers are indicated at the left. Because there were so many protein bands in the gels, the gel slices contained multiple proteins. The protein bands identified by mass spectrometric analysis after in-gel digestion of protein bands with protease are indicated on the right. Proteins that were also identified in the FLAG-DDX47-associated complex are underlined. (**b**) Silver-stained 10% SDS–PAGE gel of FLAG-DDX47-associated complexes immunoprecipitated with anti-FLAG after expression of FLAG-tagged full-length DDX47 in 293 cells. Molecular weight markers are indicated at the left. The protein bands identified by mass spectrometric analysis after in-gel digestion of protein bands with protease are indicated on the right. Proteins that were also identified in the FLAG-NOP132-associated complex are underlined. (**c**) Silver-stained 10% SDS–PAGE gel of FLAG-DDX18-associated complexes immunoprecipitated with anti-FLAG after expression of FLAG-tagged full-length DDX18 in 293 cells. Molecular weight markers are indicated at the left. The protein bands identified by mass spectrometric analysis after in-gel digestion of protein bands with protease are indicated on the right. Proteins that were also identified in FLAG-NOP132- and FLAG-DDX47-associated complexes are underlined and in bold, respectively.

immunoprecipitate NOP132-associated proteins from human 293EBNA cells expressing FLAG-tagged NOP132. Silver-stained SDS–PAGE gels of the immunoprecipitated fraction indicated that the NOP132 complexes contained many proteins spanning a wide range of molecular weights (Figure 1a, lane 2). In contrast, only three protein bands were apparent in a mock immunoprecipitate prepared from untransfected control cells (Figure 1, lane 1). These results suggest that many of the proteins immunoprecipitated from FLAG-NOP132-transfected cells represent NOP132-associated proteins.

The protein components of the NOP132 complexes were identified using mass spectrometry. Protein identification was first performed for individual bands excised from SDS–PAGE gels using in-gel digestion and matrix-assisted laser desorption ionization-time of flight mass spectroscopy. This approach identified RNA helicase DEAD/H (Asp-Glu-Ala-Asp/His) box polypeptide 47 (DDX47), ribosomal protein L3 (RPL3), glutamate-rich WD repeat protein (GRWD1), and KIAA0539 [NOP254, a possible human ortholog to yeast Npa1p (31)] as candidates for NOP132-associated proteins (Figure 1a, lane 2). A nanoscale LC-MS/MS system confirmed the presence of these proteins in the FLAG immunoprecipitates (Supplementary Table 1). A similar identification experiment was performed to isolate more complex-associated proteins using 293 cells as recipient (Figure 1a, lane 3). We found that most of the NOP132 was resistant to solubilization with our immunoprecipitation buffer, but could be more completely solubilized upon brief sonication. Thus, we briefly sonicated NOP132-transfected 293 cells and solubilized FLAG-tagged NOP132 efficiently (Figure 1a, lane 3). These experiments also identified nucleolin/NCL (yeast ortholog Nsr1), B23/NPM1, fibrillarin/FBL (Nop1), Nop5/Nop58, BRIX/BXDC2 (Brx1), putative nucleotide-binding protein estradiol-induced nuclear GTPase/GNL3 (Nug1), RNA helicase Gu/DDX21, DHX9, DDX18 (Has1), many ribosomal proteins from the large and small subunits, and other non-ribosomal proteins, most of which were found in previously characterized human pre-ribosomal ribonucleoprotein (rRNP) complexes, as candidates for NOP132-associated proteins (Figure 1a; Tables 1 and 2;

Table 1. Putative NOP132-, DDX47-, and DDX18-associated proteins

Putative function	**NOP132/NOL8**-associating proteins	**DDX47**-asssociating proteins	**DDX18**-associating proteins
Putative ribosome biogenesis proteins	DDX47, FBL, GRWD1, NCL, NPM1, WDR57, NOP254/C21orf108	BMS1L, BOP1, BXDC2, C4orf9, C20orf6, CIRH1A, DDX10, DDX24, DDX27, DDX47, EBNA1BP2, FBL, FLJ12949, FTSJ3, GNL2, GNL3, GTPBP4, GRWD1, HEATR1, HRB2, KIAA0179, KIAA0690, MKI67IP, MPHOSPH10, NCL, NOC2L, NOC3L, NOL1, NOL5A, NOP5, NOP254/C21orf108, NPM1, PDCD11, PES1, PPAN, RBM28, RRS1, RSL1D1, SART3, SDAD1, TBL3, WDR46, XRN2	DDX18, **DDX47**, **FBL**, **FLJ12949**, **GNL3**, **GTPBP4**, **HRB2**, **NCL**, **NOL1**, **NPM1**, **RSL1D1**
Ribosome subunits	RPLP0, RPL3, PRL3L, RPL4, RPL6, RPL7, RPL7A, RPL8, RPL10A, RPL13, RPL14, RPS2, RPS3, RPS3A, RSP4RPS4, RPS6, RPS8, RPSA, RSMB	RPLP0, RPL3, RPL3L, RPL4, RPL6, RPL7, RPL7A, RPL7L, RPL7L1, WUGSC:H_RG054D04.1, RPL8, RPL10, RPL10A, RPL13, RPSA, RPS2, RPS3, RPS3A, LOC146053, RPS4, RPS6, RPS8, MRPS2,MRPS9, MRPS22, MRPS28, MRPS29, MRPS34	RPLA0, **RPL3**, **RPL4**, **RPL6**, **RPL7**, **RPL7A**, **RPL8**, **RPL10A**, **RPL13**, RPL14, RPL19, **RPS2**, **RPS3**, **RPS3A**, **RPS4**, **RPS6**, **RPS8**
Putative mRNA splicing factors	ASCC3L1, CDC5L, DHX15, HNRPA0, HNRPA1, HNRPD, HNRPF, HNRPH1, HNRPH2, HNRPU, IVNS1ABP, RBMX, PRPF31, PTBP1, RBM10, SF3B1, SF3B3, SF3B4	DHX15, HNRPAB, HNRPA0, HNRPA3, HNRPC, HNRPCL1, HNRPF, HNRPM, HNRPR, HNRPU, PRPF31, RBM10, SF3B1, SFRS10, SNRPA1, SNRPB2, SNRP70	CDC5L, **DHX15**, **HNRPAB**, HNRPA2B1, HNRPD, **HNRPF,** HNRPH1, HNRPH2, **HNRPM**, **HNRPR**, HNRPQ, **HNRPU**, HNRPUL1, IVNS1ABP, **PRPF31**, **RBM10**, **SF3B1**, SF3B3, SNRPN, U2AF2
Heat shock	CCT6A, CDC37, DNAJA1, HSPA1L, HSPA2, HSPA4, HSPA4L, HSPA5, HSPA6, HSPCA, HSPD1, HSPH1	HSPA1L, HSPA6, HSPA9B, HSPD1	**HSPA1L**, HSPA5, **HSPA6**, **HSPA9B**, HSPCA, **HSPD1**
Chromatin binding	HIST1H1C	H1FX, H1F0, HIST1H1C, H2AFY, H2AFY2	H1FX, **HIST1H1C**
Signal transduction	JAK1, MAP3K7IP1		CENTB2-ARF GAP. MAP3K7, MAP3K7IP1.
Transcription	CSDA, DHX9, E2F7, ILF3, P53, SSB, TAF4	AATF, ABT1, BCLAF1, C1orf107, CEBPZ, CSDA, CTCF, DHX9, FLJ10774, ILF2, MYBBP1A, PURA, PWP1, RARA, YBX1, ZFR	**DHX9**, **MYBBP1A**, ILF3, SSB, YBX1
Translation	DDX21, EEF1A , EEF1G, EIF4B, WARS	DDX21, DDX50, EIF3S10, EIF4B, IMP1IGF2BP1, IGF2BP2IMP2, IGF2BP3IMP3, IGF2BP4IMP4, LARP1, PABPC4	GRSF1, **DDX21**, EIF2B, **EIF4B**
Filament	ACTS, CLASP2, TUBA1, TUBA6, TUBB TUBB2A, TUBB4, TUBB6, VIM	FLNA	TUBB, TUBA3, TUBB2C
Transport	KPNA3, KPNA4, KPNB1	KPNA2	
Protein degradation		FAF-X, FAF-Y, UBR2	
Others and unknown	ANKFY1, FHL2, KIAA0133, LOC144097, C14orf150	C14orf120, FLJ20758, HP1BP3, KIAA0020, LYAR, MATR3, MOV10, NOL10, SLC25A6, PABPC1	PRPSAP2, ANKFY1, LOC144097, OTUD4, **PABPC1**

Gene names according to HUGO nomenclature. DDX47- and DDX18-associated proteins that were also identified in FLAG-NOP132-associated complexes are underlined. DDX18-associated proteins that were also identified in FLAG-DDX47-associated complexes are in bold.

Supplementary Table 1) (4,30,32). In addition, the FLAG immunoprecipitates in FLAG-NOP132-expresssing cells contained many splicing factors, suggesting that NOP132 might also be involved in pre-mRNA splicing. This is consistent with our previous observation that NOP132 co-localizes with proteins such as Clk-1 and RNPS1 located in nuclear speckles (15). P53, a tumor suppressor, was repeatedly identified in NOP132 complexes (Table 1 and Supplementary Table 1) and was also detected in NOP132 complex by western blotting (data not shown). RRAG A was not detected in the NOP132 complex, however. This finding might be the result of a transient interaction or because RRAG A is a minor component of the NOP132 complex and consequently below the limit of detection of this experiment.

Among the proteins identified, DDX47, which was repeatedly identified, and DDX18, which was identified once but belongs to a group of proteins similar to DDX47, were used for reciprocal immunoprecipitation experiments. The associated proteins were identified from SDS–PAGE gels as described above (Figures 1b, c and 2b) and are summarized in Table 1. One hundred and eight proteins associated with DDX18 and 119 proteins associated with DDX47 were identified by nano-LC-MS/MS analysis after Lys-C digestion (Supplementary Table 1). Analysis of these proteins indicated that the two complexes share 37 large subunit ribosomal proteins, 23 small subunit ribosomal proteins, and 41 non-ribosomal proteins in common, demonstrating their similarity in protein composition. DDX47 was found in the DDX18

Table 2. Putative NOP132-, DDX47-, and DDX18-associated trans-acting factors involved in ribosome biogenesis

Putative function	**NOP132**/**NOL8**-associating proteins	**DDX47**-asssociating proteins	**DDX18**-associating proteins
18S rRNA (40S subunit)	DDX47 (RRP3), FBL(NOP1), NCL(NSR1)	BMS1L(*BMS1*), C4orf9(*NOP14*), C20orf6(*ESF1*), CIRH1A(*UTP4*), DDX47, FBL, FLJ12949 (*KRI1*), HEATR1 (*UTP10*), HRB2(*KRR1*), MPHOSPH10 (*MPP10*), NCL, NOP5 (*NOP5*), PDCD11 (*RRP5*), SART3(*NSR1*), TBL3(*UTP13*), WDR46(*UTP7*)	DDX18 (*HAS1*), **DDX47**, **FBL**, **NCL**, **FLJ12949**
28S rRNA (60S subunit)	DDX47, GRWD1(*RRB1*), NPM1, WDR57 (*RSA4*)	BOP1(*ERB1*), BXDC2 (*BRX1*), DDX24 (*MAK5*), DDX27(*DRS1*), DDX47, EBNA1BP2(*EBP2*), FTSJ3(*SPB1*), GNL2 (*NOG2*), GNL3 (*NUG1*), GTPBP4(*NOG1*), GRWD1, KIAA0179 (*RRP1*), MKI67IP(*NOP15*), NOC2L(*NOC2*), NOC3L(*NOC3*), NOL1(*NOP2*), NOL5A (*SIK1*), NPM1, PES1 (*NOP7*), PPAN (*SSF1*), RBM28 (*NOP4*), RRS1(*RRS1*), RSL1D1(*CIC1*), XRN2(*RAT1*)	**GNL3**, **GTPBP4**, **NOL1**, **NPM1**, **RSL1D1**
Other	NOP254/C21orf108	DDX10 (HCA4), KIAA0690(RRP12), NOP254/C21orf108, SDAD1(*SDA1*)	

Gene names according to HUGO nomenclature. DDX47- and DDX18-associated proteins that were also identified in FLAG-NOP132-associated complexes are underlined. DDX18-associated proteins that were also identified in FLAG-DDX47-associated complexes are in bold letter. Potential Yeast homologs are indicated in parentheses.

complex but, we did not detect DDX18 in the DDX47 complex (Figure 1b, Table 1 and Supplementary Table 1), suggesting that a major portion of the DDX47 complexes is present in human cells without DDX18 or expression level of DDX18 is low. The analyses further indicated that 32 non-ribosomal proteins, including probable trans-acting factors involved in ribosome biogenesis, such as nucleolin/NCL (Nsr1), B23/NPM1, putative nucleotide binding protein estradiol-induced nuclear GTPase/GNL3 (Nug1), RNA helicase Gu/DDX21, and DHX9, found in the NOP132-associated complex were also found in DDX18- and DDX47-associated complexes (Table 1 and Supplementary Table 1). In addition most of the ribosomal proteins found in the NOP132-associated complexes were also present in the in DDX18- and DDX47-associated complexes. The overlap of proteins present in all three complexes suggests functional similarity among these complexes in human ribosome biogenesis.

Among the non-ribosomal proteins we identified, karyopherins α3, α4, and β1 were present only in NOP132-associated complexes (Table 1 and Supplementary Table 1). Of these, karyopherin α3 interacted with NOP132 even after-RNase treatment (data not shown and Supplementary Table 1). Because karyopherin α3 binds to the NLS and is a transporter for nuclear proteins containing a NLS (33), it might have a role in the transport of NOP132 from the cytoplasm to the nucleus. Similarly, karyopherin α2 was present in the DDX47-associated complex (Figure 1b, Table 1), suggesting that it might be a nuclear transport factor for DDX47.

Association of NOP132 with DDX47 and DDX18

Despite the fact that DDX18 and DDX47 were detected in FLAG-NOP132-associated complexes by nano-LC-MS/MS analysis, NOP132 was not found in either FLAG-DDX18- or FLAG-DDX47-associated complexes (Figure 1b and c; Table 1). To confirm the association of NOP132 with DDX18 and DDX47, we performed co-immunoprecipitation experiments using cell extracts prepared from 293 cells transfected with NOP132 and either FLAG-tagged DDX18 or FLAG-tagged DDX47 (Figure 2a). These experiments confirmed that NOP132 can associate with both DDX18 and DDX47. The association of NOP132 with DDX47 and DDX18 was decreased significantly by RNase treatment (Figure 2a, lanes 7 and 9), suggesting that their interaction is dependent on RNA. Similarly, most of the NOP132-, DDX47-, and DDX18-associated proteins were released by RNase treatment (Figure 2b, lanes 2, 4 and 6), suggesting that RNAs are crucial for complex formation. However, several proteins remained associated with FLAG-NOP132 or FLAG-DDX47 after RNase treatment, as shown in Figure 2b (lanes 2 and 4).Other protein bands in Figure 2b (lanes 2, 4 and 6) were identified to be NOP132, DDX47, DDX18 or background proteins (identified from a control experiment of 293 cells transfected with a FLAG vector) (Figure 2b, lanes 8 and 9). We also examined the association using purified GST-DDX47, GST-DDX18 and GST-GRWD1 with NOP132 synthesized in baculovirus in an *in vitro* binding assay and demonstrated that NOP132 bound both DDX47 and DDX18 *in vitro* (Figure 2c). A very small but significant amount of NOP132 was detected when a small amount of GST-DDX18 was used to pull down NOP132. We were unable to use larger amounts of GST-DDX18 because most of the *E.coli*-produced GST-DDX18 was insoluble. Although GRWD1 was detected in NOP132-associated complexes that were isolated from cell lysates, GST-GRWD1 was not able to bind NOP132 *in vitro* (Figure 2c, lane 2), suggesting that the association of GRWD1 with NOP132 occurs indirectly. Alternatively, it could require a co-factor that was not present in this *in vitro* system. Control GST did not pull down NOP132 (Figure 2c, lane 1). Because NOP132 bound FLAG-DDX47 *in vitro*, the failure to identify NOP132 in the DDX47-associated complexes by mass spectrometry suggests that their association is transient or that NOP132 is only a minor component of DDX47-associated complexes.

Next, we examined whether NOP132 co-localized with DDX47, DDX18, RPL3, or KIAA0539/NOP254/C21orf108

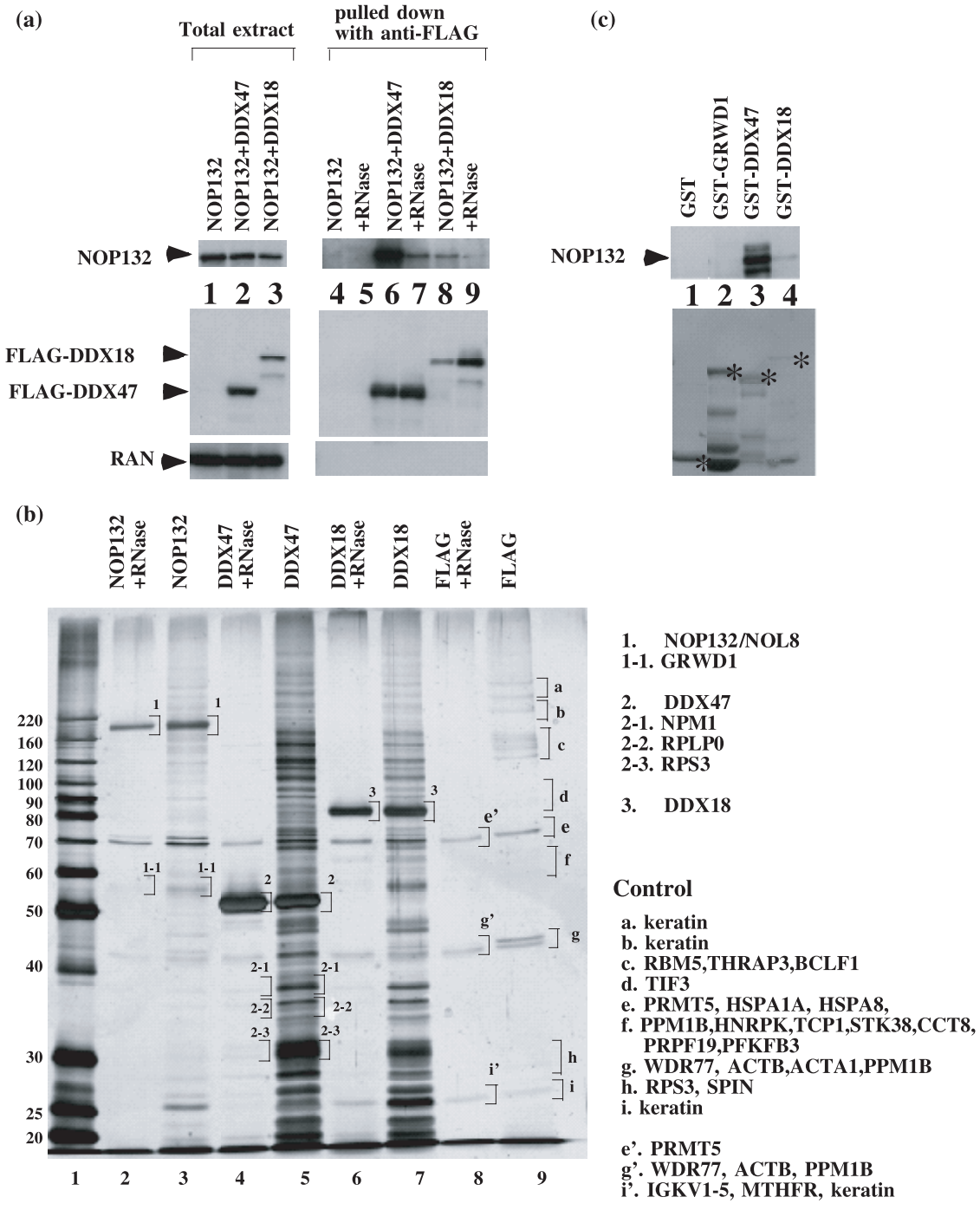

Figure 2. Association of NOP132 with DDX18 and DDX47. (**a**) 293 cells were transfected with NOP132 and either FLAG-tagged DDX18 or FLAG-tagged DDX47. Cell lysates were prepared and used for immunoprecipitation with anti-FLAG as described (15). Total cell protein (2% input) (lanes 1–3). Immunoprecipitates (lanes 4–9). Proteins were detected with anti-NOP132N (upper panels), anti-FLAG (middle panels) or a RAN antibody against the nuclear protein RAN as a loading control (lower panels). Lane 4, control immunoprecipitate (NOP132 transfected); lane 5, control immunoprecipitate (NOP132 transfected) treated with ribonuclease; lane 6, immunoprecipitation with anti-FLAG of FLAG-tagged DDX47 lysate; lane 7, immunoprecipitation with anti-FLAG of FLAG-tagged DDX47 lysate treated with ribonuclease; lane 8, immunoprecipitation with anti-FLAG of FLAG-tagged DDX18 lysate; lane 9, immunoprecipitation with anti-FLAG of FLAG-tagged DDX18 lysate treated with ribonuclease. (**b**) 293 cells were transfected with either FLAG-NOP132, FLAG-DDX18, or FLAG-DDX47. Silver-stained 10% SDS–PAGE gel of FLAG-NOP132-, FLAG-DDX47-, or FLAG-DDX18-associated complexes immunoprecipitated with anti-FLAG. Lane 1, molecular weight marker; lane 2, NOP132-associated proteins treated with ribonuclease; lane 3, NOP132-associated proteins; lane 4, DDX47-associated proteins treated with ribonuclease; lane 5, DDX47-associated proteins; lane 6, DDX18-associated proteins treated with ribonuclease; lane 7, DDX18-associated proteins; lane 8, control FLAG tag-associated proteins treated with ribonuclease; lane 9, control FLAG tag-associated proteins. Proteins which were identified by mass spectrometry are shown at the right of the gel image. (**c**) Baculovirus-produced NOP132 was mixed with GST (lane 1), GST-GRWD1 (lane 2), GST-DDX47 (lane 3), or GST-DDX18 (lane 4) bound to the glutathione-Sepharose-4B beads. Bound NOP132 was detected by western blotting using anti-NOP132N (upper panel). GST-fusion proteins stained with Coomassie brilliant blue are shown in the lower panel. Asterisks indicate the positions of the GST-fusion proteins.

in hamster cells. Each of the four proteins was fused with EGFP and transfected with DsRed-NOP132 into BHK21 cells. Fluorescence microscopy examination revealed that these four proteins co-localized with NOP132 in the nucleolus (Figure 3a). Consistent with this finding, DDX47 localizes to the nucleolus under normal growth conditions (34). Surprisingly, NOP132 co-localized with EGFP-RPL3, which was expected to be localized mainly in the cytoplasm. However, Andersen *et al*. (35) reported that RPL3 was detected in a proteomic analysis of the human nucleolus. Thus, it is likely that NOP132 co-localized with a nucleolar fraction of RPL3. We also observed that DDX18 and KIAA0539 localized to the nucleolus (Figure 3a and b). We believe that KIAA0539, which has some similarity to yeast Urb1p/Npa1, is a novel nucleolar protein (Figure 3a), and therefore named it NOP254, based on its nucleolar localization and its molecular weight of 254 kDa. In addition, we confirmed the nucleolar localization of endogenous DDX47 and DDX18 by immunostaining using affinity purified polyclonal antibodies against each protein (Figure 3b).

Roles of NOP132 and DDX47 in pre-rRNA processing

To examine the roles of NOP132 and its associated proteins in pre-rRNA processing, RNAi experiments of NOP132 and DDX47 were carried out. After introduction of the siRNAs to the cells, total RNA was purified and used for northern blotting analysis (Figure 4a). RNAs from same number of cells (about 4000 cells) were loaded onto the gel to compare the amount of rRNAs and rRNA precursors in wild type, NOP132 RNAi-treated and DDX47 RNAi-treated cells. Downregulation of NOP132 slightly decreased 18S rRNA and rRNA precursors, including 45S/47S rRNA, suggesting that NOP132 have a role in rRNA processing. Likewise, downregulation of DDX47 also decreased the amounts of mature rRNAs and rRNA precursors in HeLa cells, suggesting that DDX47 is also involved in rRNA production. We cannot rule out possibility that some pre-rRNAs are degraded. We observed that the total amount of RNA per cell decreased on average about 30% in NOP132-downregulated cells and about 40% in DDX47-downregulated cells in three separate cell samples. It could be possible that this decrease in RNA was caused by a kind of stringent control [reviewed in (36)], which might be induced by interruption of rRNA processing by downregulation of NOP132 or DDX47. Figure 4b shows that addition of NOP132 siRNA and DDX47 siRNA downregulated expression of their respective proteins. The amount of actin mRNA was also decreased in these cells (Figure 4a, lowest panel), suggesting that DDX47 might function in mRNA splicing. Consistently, many proteins involved in mRNA splicing were found in DDX47-associated complexes (Table 1). Next, we examined the association of DDX47 with rRNA precursors by transfecting 293 cells with FLAG-tagged DDX47. RNAs from the FLAG-DDX47-expressing cells were purified by immunoprecipitation with anti-FLAG and used for northern blotting analysis (Figure 4c). FLAG-DDX47 associated with 32S, 30S, 26S, 17S rRNA precursors and 18S, 5.8S and 28S rRNAs, suggesting that DDX47 is involved in early stages of pre-rRNA processing, probably after the primary rRNA transcript is synthesized (Figure 4d). Because DDX47 associated with both 30S and 32S rRNA precursors, DDX47 might be involved in 18S and 28S rRNA maturation. Consistent with this, DDX47 associated with both 18S and 28S rRNA maturation proteins, as shown in Table 2, in which the functions of human proteins were

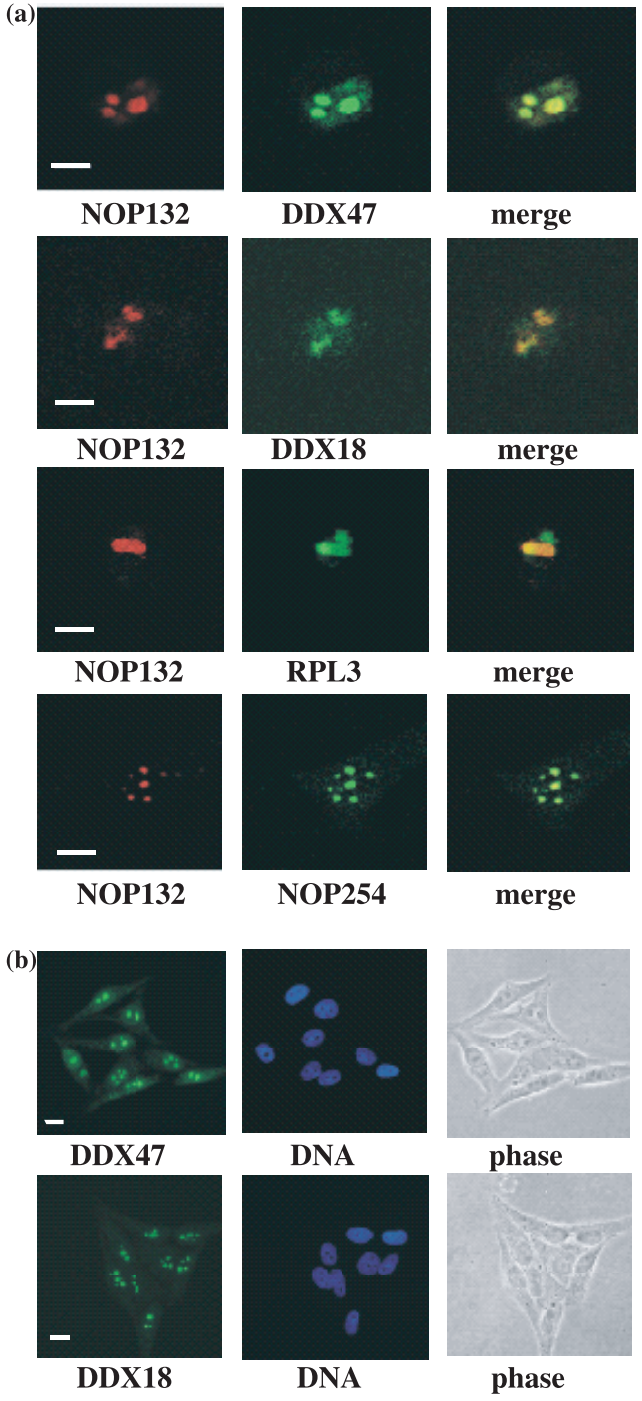

Figure 3. Co-localization of NOP132 with DDX47, DDX18, RPL3, and NOP254 in the nucleolus. (**a**) BHK21 cells were transiently cotransfected with DsRed-NOP132 (red) and DDX47-EGFP, DDX18-EGFP, RPL3-EGFP, or KIAA0539/NOP254-EGFP (green). The cells were fixed and processed for confocal microscopy imaging as described in the Materials and Methods. Scale bars, 10 μm. (**b**) HeLa cells were fixed and immunostained with affinity purified rabbit polyclonal anti-DDX18 or anti-DDX47 followed by fluorescein-isothiocyanate-conjugated anti-rabbit secondary antibody. DNA was stained with Hoechst dye. Phase images are shown in the right panels.

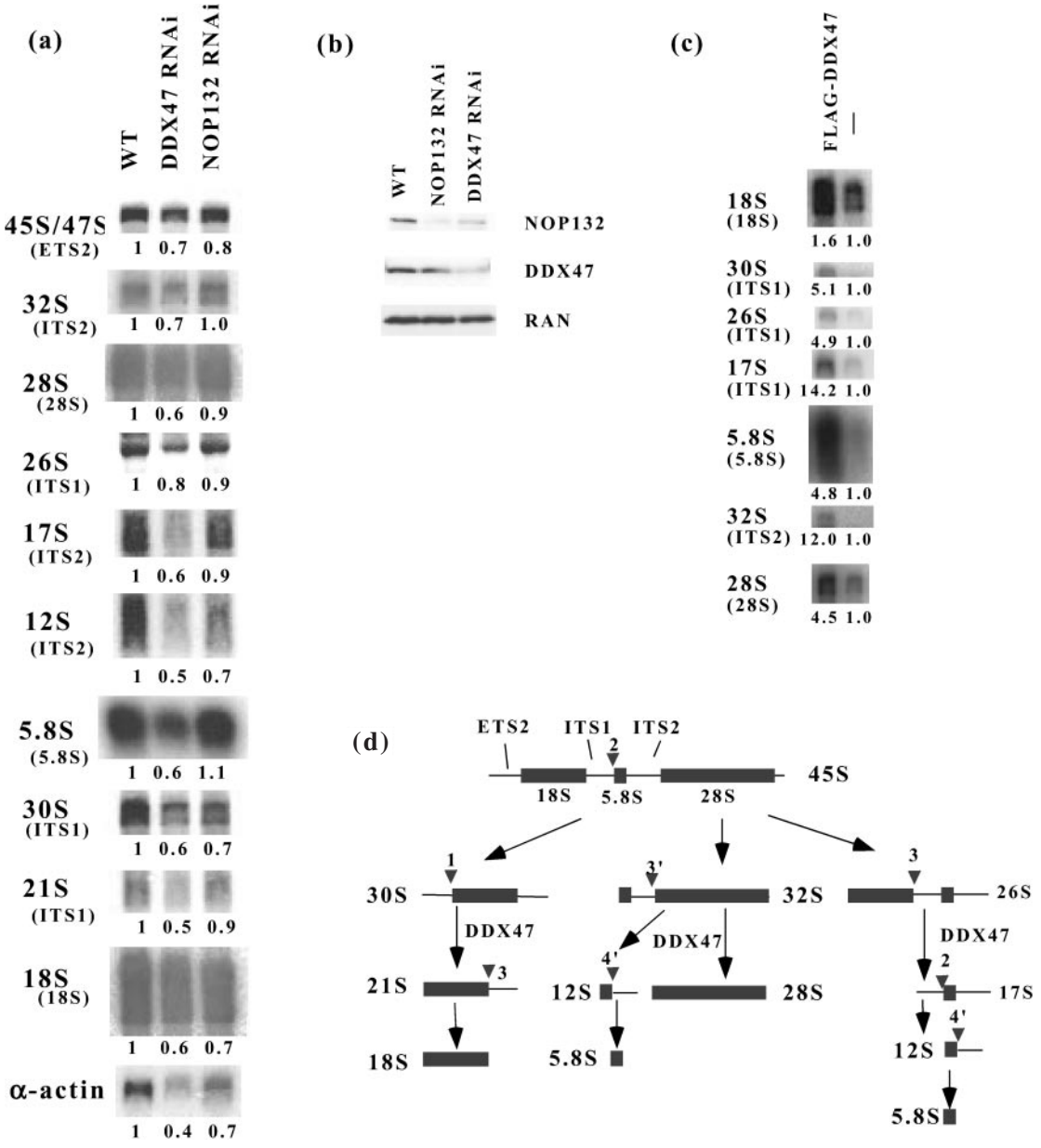

Figure 4. Association of DDX47 with pre-rRNAs. (**a**) HeLa cells were transiently transfected with two dsRNAs for each RNAi experiment as described in the Materials and Methods. WT, Control fruit fly luciferase oligonucleotide; DDX47 RNAi, oligonucleotides DDX47-1 and -2; NOP132 RNAi, oligonucleotides NOP132-B and -C. After transfection for 1 d, total RNAs were purified and processed for Northern blot analysis using ITS1, ITS2, 28S, 18S, 5.8S, or α-actin DNAs as probes (shown in parentheses). RNA from control (WT), NOP132 RNAi-treated, and DDX47 RNAi-treated cells was electrophoresed on a formaldehyde agarose gel as described in the Materials and Methods. Radioactivity in each lane was measured using the Fuji BAS2500 Image Analyzer (Fuji Photo Film Co. Ltd, Japan). Relative radioactivity of each rRNA or rRNA precursor is shown at the bottom of the panels. (**b**) Proteins from the siRNA-treated cells were isolated and processed for western blotting analysis using anti-NOP132N, anti-DDX47, or anti-RAN as a loading control. (**c**) 293 cells were transiently transfected with FLAG- DDX47. After transfection for 2 d, a cell lysate was prepared and the DDX47-associating complex was purified with anti-FLAG. RNA was purified from the immunoprecipitate and processed for Northern blot analysis using ITS1, ITS2, 28S, 5.8S, or 18S oligonucleotide probes. As a control, an untransfected 293 cell lysate was prepared and processed as above. Relative radioactivity of each rRNA or rRNA precursor is shown at the bottom of the panels. (**d**) Schematic representation of the pre-rRNAs detected in the Northern blots. Possible points where DDX47 might act are indicated in the figure. The pre-rRNA cleavage sites (1- 3, 3′, 4′) are indicated by arrowheads.

deduced from the known functions of their yeast orthologs. We also examined the association of FLAG-tagged NOP132 with the rRNA precursors; however, we did not detect a significant amount of rRNA precursor (data not shown). This might be the result of a transient association of NOP132 with pre-rRNAs. As a control, we analyzed a non-tagged control strain in parallel in Figure 4c.

Proper nucleolus localization of DDX47 by NOP132

Inhibition of rRNA synthesis by actinomycin D results in re-localization of DDX47 from the nucleolus to the entire nucleus, along with other nucleolar proteins (37). Although DDX47 is localized exclusively in the nucleolus in quiescent cells, an anchoring protein for DDX47 in the nucleolus has not been identified. We examined the possibility that

NOP132 acts as a nucleolar anchoring protein for DDX47. Reduction of NOP132 expression by siRNA caused DDX47 to localize to the nucleolar periphery, probably in the granular component (GC) region (Figure 5a). This result suggests that DDX47 can still be recruited to the nucleolus in the absence of NOP132 but that NOP132 is required for retention of DDX47 in the fibrillar center (FC) and/or dense fibrillar components (DFC) region of the nucleolus. When actinomycin D was applied to HeLa cells for 8 h, DDX47 localized uniformly throughout the nucleus (Figure 5b), suggesting that recruitment and retention of DDX47 to the nucleolus requires active transcription (Figure 5c). To confirm that NOP132 plays a role in binding and recruiting DDX47 to the FC or DFC region of the nucleolus, we used a FLAG-tagged NOP132 coiled-coil domain fragment (FLAG-Coil), which contains the minimum region required to interact with DDX47 (see Figure 7) but lacks the NLS; this form of NOP132 localized mainly in the cytoplasm (Figure 5e). When EGFP-DDX47 was expressed alone in 293 cells, most of the EGFP-DDX47 localized to the nucleolus (Figure 5f). When FLAG-Coil was transiently cotransfected with EGFP-DDX47 into 293 cells, EGFP-DDX47 distributed evenly in the nucleus and FLAG-Coil was distributed in both the cytoplasm and the nucleus (Figure 5d, upper and lower panels). In some cells in which FLAG-Coil expression was low and DDX47 expression was high, the FLAG-Coil fusion mutant NOP132 protein was localized in the nucleus (Figure 5d, middle panels). Thus, it appears that the subcellular localization of EGFP-DDX47 was influenced by the relative expression levels of the FLAG-Coil protein and EGFP-DDX47. Together, these results suggest that NOP132 is required for DDX47 to localize in the nucleolar-organizing region during ribosome biogenesis.

Next, we identified the DDX47 region responsible for subcellular localization using a series of EGFP-fused DDX47 deletion proteins in BHK21 cells (Figure 6a and b). Nuclear export or cytoplasmic retention signals were found to reside between amino acid residues 50 and 100. A NLS in the C-terminal region was found to reside between residues 400 and 456. A nucleolar localization region was predicted to be between amino acid residue 200 and the C terminus because the EGFP fusion protein containing the region from residue 200 to the C terminus had a nucleolar staining pattern but the EGFP fusion protein containing the region from residue 300 to the C terminus had lost its nucleolar localization (Figure 6a). A search for known protein sequence motifs was performed with the Conserved Domain Database (CDD) (38); it revealed that the region from residue 200 to the C terminus of DDX47 contains the helicase superfamily C-terminal domain (HELICc) motif, which is found in a wide variety of helicases and helicase-related proteins. To examine whether the region that determines the nucleolar localization of DDX47 is the region that interacts with NOP132, we performed a yeast two-hybrid assay using DDX47 as the bait and found that the same region of DDX47, residue 200 to the C terminus, was also responsible for binding to NOP132 (Figure 6a and c). Thus, the NOP132-interacting region of DDX47 also functions as a nucleolar localization signal. This result is consistent with the idea that NOP132 is required for the proper nucleolar localization of DDX47. In contrast, NOP132 siRNAs did not affect the nucleolar localization of DDX18 (data not shown), suggesting that proteins other than NOP132 determine the nucleolar localization of DDX18.

NOP132 coiled-coil structure is responsible for binding to both DDX18 and DDX47

We used a yeast two-hybrid assay to further examine the region of NOP132 responsible for binding to DDX18 and DDX47 (Figure 7a and b). Serial deletion constructs of NOP132 were constructed in the vector pACT2 (Figure 7b) and subjected to β-galactosidase filter assays using DDX47 or DDX18 as bait. The results indicated that the region of NOP132 containing two coiled-coil structures was responsible for binding to both of the DDX proteins. The coiled-coil structure is known to mediate protein–protein interactions and subunit oligomerization [see review in (39)]. Because the region of DDX47 that interacts with NOP132 contains a HELICc motif (as described above), it is likely that the NOP132 coiled-coil motif interacts directly with the DDX47 HELICc motif. DDX18 also contains a HELICc motif at the C terminus, has high sequence similarity to DDX47 in that region, and interacts with NOP132 (Figure 7c). The HELICc motif of DDX18 might also directly interact with the coiled-coil motif of NOP132. Because other DDX family proteins have an amino acid sequence similar to the HELICc motif, we examined the possibility that the other DDX family proteins also bind to NOP132. We performed yeast two-hybrid assays on DDX3, DDX5, DDX21, and DDX49; however, none of these DDX proteins interacted with NOP132 (data not shown), suggesting that the interaction with NOP132 is specific to DDX47 and DDX18.

DISCUSSION

NOP132 and DDX47 are involved in human ribosome biogenesis

The present study demonstrates that NOP132 physically interacts and co-localizes with DDX47 and DDX18. Their associated complexes contained a number of proteins found in previously reported human pre-rRNP complexes (4,30–32). We also found that FLAG-tagged DDX47 associated with pre-rRNA precursors and RNAi-mediated downregulation of NOP132 resulted in mislocalization of DDX47. These results, coupled with the nucleolar localization of NOP132 and DDX47, strongly suggest that NOP132 and DDX47 are involved in human ribosome biogenesis cooperatively.

The yeast ortholog of human DDX47 is Rrp3 (identity, 57%), which plays a role in the cleavage of A0 (the 5′ external transcribed spacer), A1 (the 5′ end of the 18S rRNA) and A2 (located 1.9 kb away in ITS1) and in the processing of pre-rRNA, and is required for 18S rRNA production in yeast cells (40). Although it was reported that the yeast ortholog of human DDX47 is Prp3 with 56% identity (21), we did not find such identity between these proteins. DDX18 also potentially has several roles in early ribosome biogenesis: it is similar to yeast Has1 (identity, 60%), which is a component of 90S and pre-60S ribosomal particles (41), is an essential trans-acting factor involved in 40S ribosomal subunit biogenesis (42), is a direct target of MYC

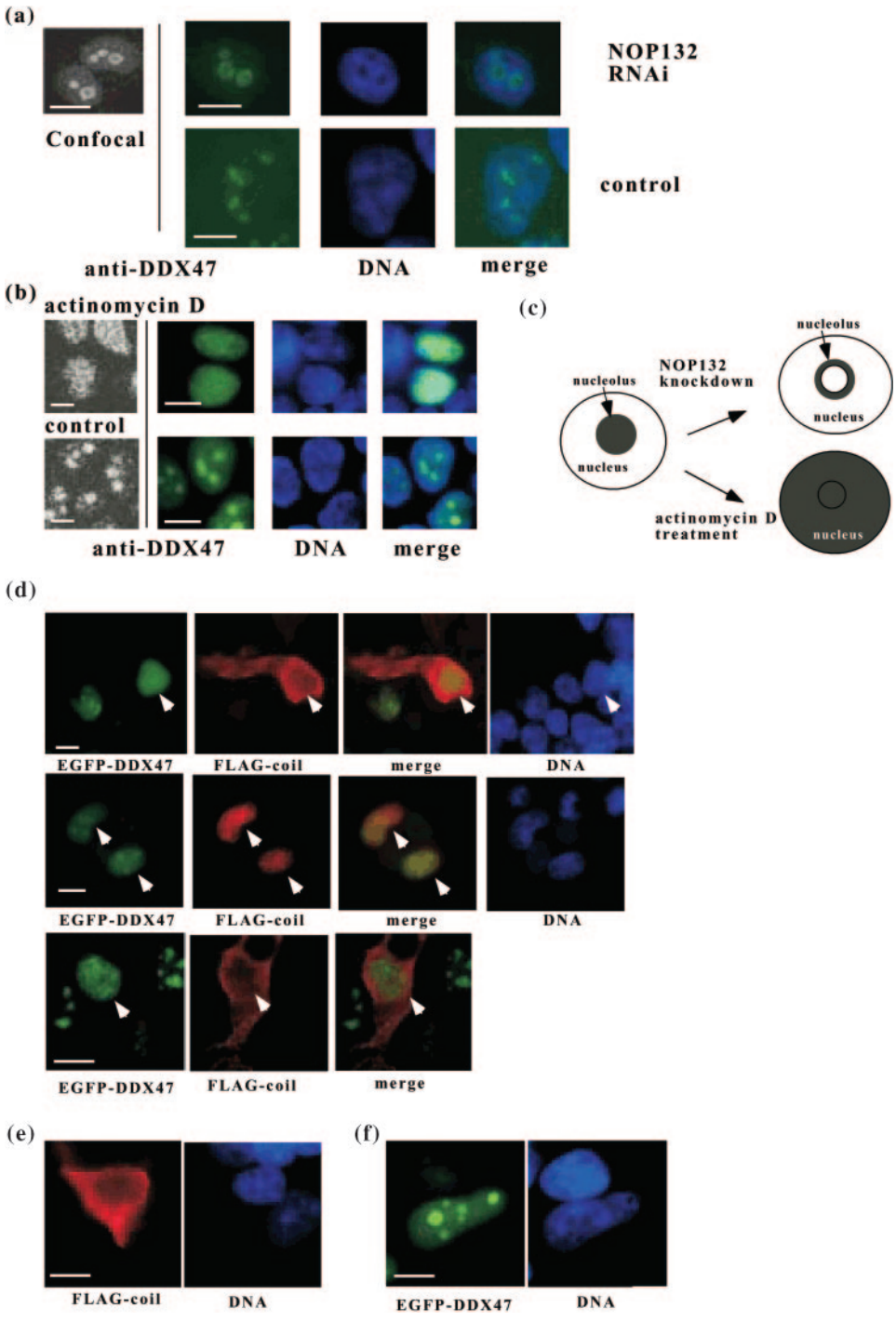

Figure 5. NOP132 is required for DDX47 to properly localize to the nucleolus. Localization of DDX47 by anti-DDX47 immunofluorescence in HeLa cells treated with NOP132 siRNAs to reduce expression of NOP132. Control cells were transfected with luciferase siRNA duplex. (**a**) NOP132 RNAi in HeLa cells (upper panels). Control luciferase RNAi in HeLa cells (lower panels). Confocal images were taken with the Olympus laser-scanning confocal microscope LSM-GB200 system (left panel). DNA was stained with DAPI. Merge images of DDX47 and DNA are shown in the rightmost panels. Fluorescence images were taken with the Zeiss Axiophot microscope (right panels). Scale bars, 10 μm. (**b**) HeLa cells were treated without (control, lower panels) or with 5 μg/ml actinomycin D for 8 h (upper panels) and then immunostained with anti-DDX47 and stained with DAPI. Left panels, confocal fluorescence microscopy. Right panels, fluorescence microscopy. (**c**) A schematic model of the change in the localization of DDX47. In the untreated state, DDX47 (in black) is localized to the nucleolus. (**d**) 293 cells were transiently cotransfected with vectors carrying EGFP-DDX47 and FLAG-NOP132 coiled-coil domain minus a NLS (residues 667–960; FLAG-Coil). The cells were fixed and stained with anti-FLAG followed by Alexa Fluor 594-goat anti-mouse IgG. Upper and middle panels, fluorescence microscopy; lower panels, confocal fluorescence microscopy. Arrowheads indicate cells in which the EGFP-DDX47 protein distributed evenly in the nucleus. DNA was stained with Hoechst dye. (**e**) 293 cells were transiently transfected with the NOP132 FLAG-Coil vector. The cells were fixed and stained with FLAG monoclonal antibody and then with Alexa Fluor 594-goat anti-mouse IgG. DNA was stained with Hoechst dye. Fluorescence images were taken with the Zeiss Axiophot microscope. (**f**) 293 cells were transiently transfected with EGFP-DDX47 vector. DNA was stained with Hoechst dye. Fluorescence images were taken with the Zeiss Axiophot microscope.

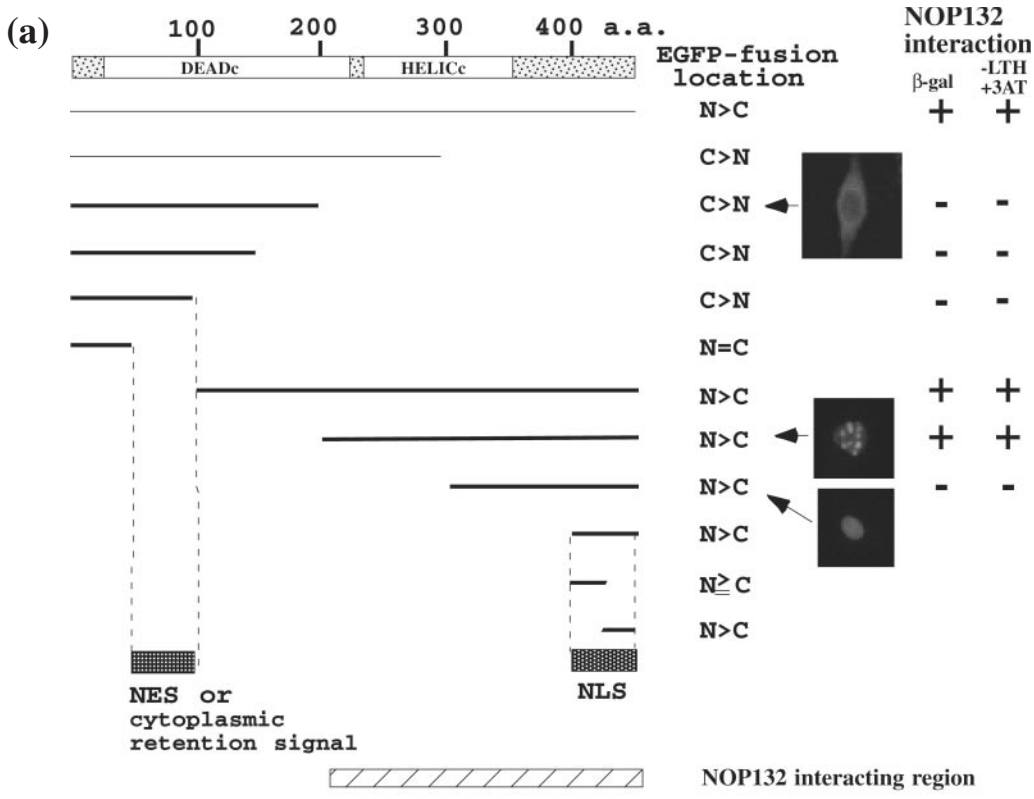

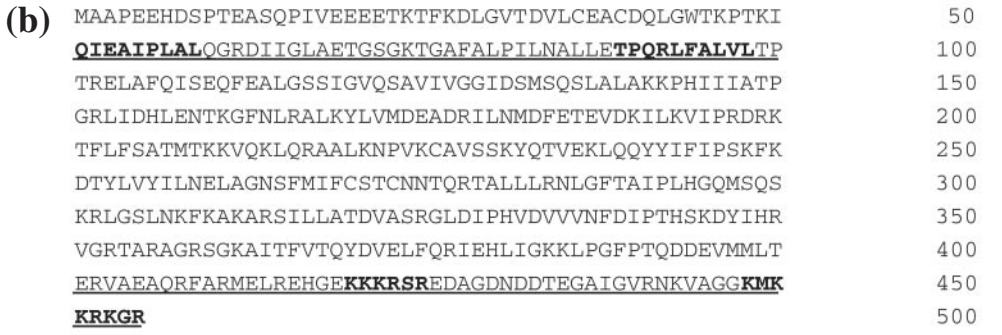

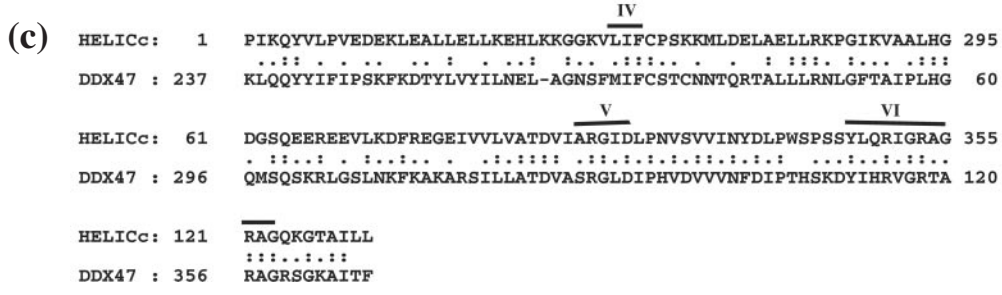

Figure 6. Analysis of regions responsible for subcellular localization of DDX47. (**a**) Serial deletion constructs of EGFP-fused DDX47 were used to transfect BHK21 cells. Subcellular localization of all constructs was determined by fluorescence microscopy. Representative fluorescence images are shown. Interaction of DDX47 deletion constructs with NOP132 was determined using two different yeast two-hybrid read-outs, a chromogenic β-galactosidase assay and a colony growth assay, and the results are shown at the far right. Domains: DEADc, CDD accession no. cd00268 (38); HELICc, CDD accession no. cd00079. Abbreviations: N, nucleus/nucleolus; C, cytoplasm; NES, nuclear export signal; NLS, nuclear localization signal; +, yeast two-hybrid interaction between the DDX47 deletion construct and NOP132; −, no interaction. Hatched box indicates the NOP132-interacting region. N, nucleus; C, cytoplasm. (**b**) DDX47 amino acid sequence is shown indicating possible NES and NLS regions (underlined) and motifs (bold). (**c**) Sequence alignment of the DDX47 and HELICc motifs. Conserved RNA helicase DEAD-box motifs IV, V, and VI are indicated (48). Two dots indicate identity and a single dot indicates chemically similar amino acids.

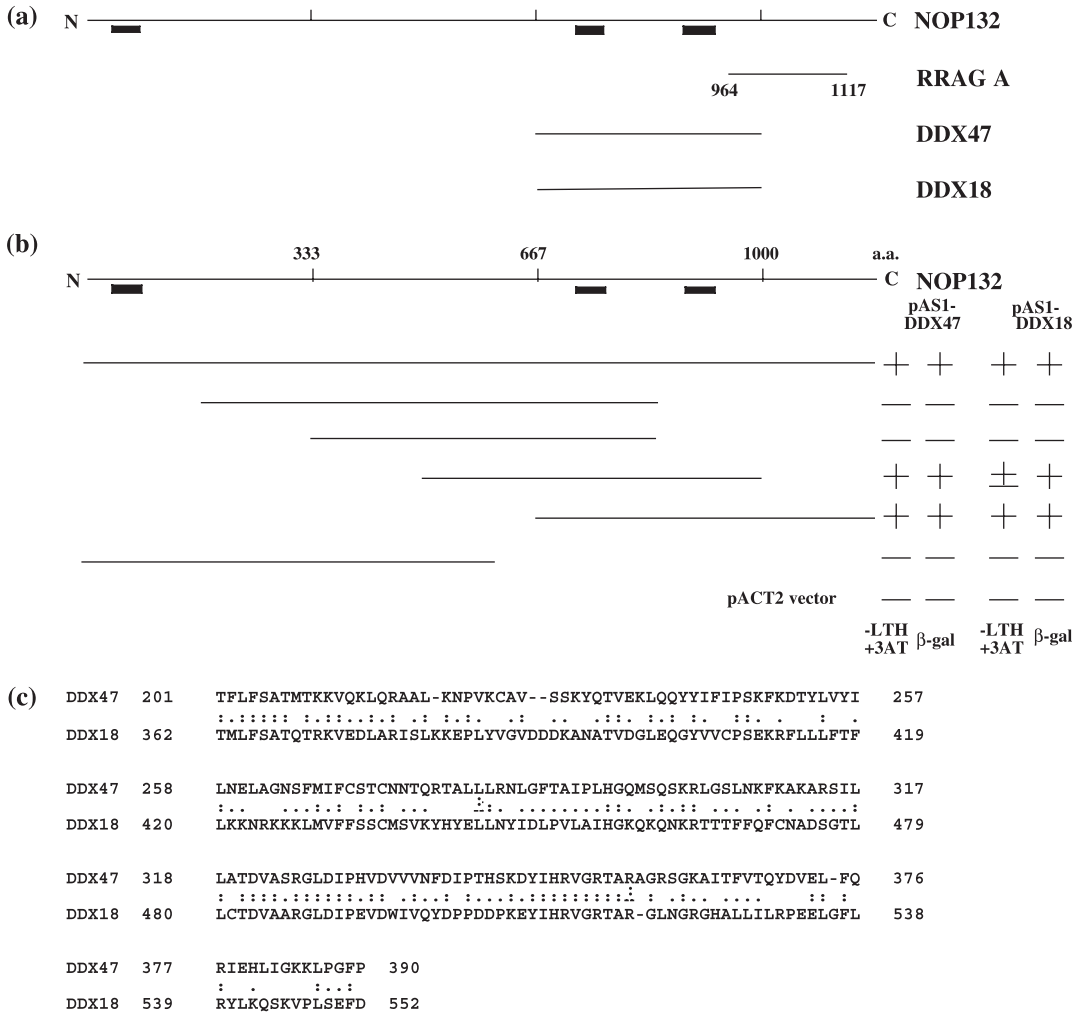

Figure 7. Determination of NOP132-interacting region of DDX47. (**a**) Summary of the region of NOP132 that associates with DDX47 and DDX18. The three coiled-coil structures are shown as black bars. (**b**) Deletion constructs of NOP132 in the vector pACT2 were examined for their interaction with DDX47 or DDX18 in the vector pAS1 using a yeast two-hybrid assay. Right panels show the results of the β-galactosidase filter assay and colony growth assay. β-gal activity indicates that an interaction had occurred. Abbreviations: + yeast two-hybrid interaction between NOP132 deletion construct and DDX47 or DDX18; +/− weak interaction; − no interaction. (**c**) Sequence alignment of the C terminus of DDX18 and DDX47 showing 37.3% identity between these proteins. Two dots indicate identity and a single dot indicates chemically similar amino acids.

in transcription (43), and is essential for growth (44). Because both Has1 and Rrp3 are essential for growth and are involved in rRNA production, DDX18 and DDX47 might have similar functions in mammalian cells. We observed that FLAG-tagged DDX47 interacts with 30S and 32S pre-rRNAs, suggesting that DDX47 is involved in early steps in pre-rRNA processing. It is likely that a main role of DDX47 could be in 60S ribosome subunit assembly, because DDX47 associates more efficiently with pre-rRNAs from 26S to 5.8S pathway as shown in Figure 4c.

RNase treatment released most of the proteins of the NOP132-, DDX47-, and DDX18-associated complexes, demonstrating that NOP132-, DDX47-, and DDX18-associated complexes contain RNAs, which could act as assembly factors. Because DDX47 and DDX18 belong to the DEAD-box RNA helicase family, it is likely that these proteins directly bind to RNAs that link to other proteins. NOP132 also has an RNA binding motif in its amino terminal region that can bind RNAs *in vitro* (T.Sekiguchi *et al*. unpublished data) and thus may directly bind to RNAs. Association of NOP132 with DDX47 or DDX18 was also dependent on RNA, as shown in Figure 2a, although we cannot rule out the possibility that NOP132 directly associates with either DDX47 or DDX18.

A possible role for NOP132 in proper nucleolus localization of DDX47 during ribosome biogenesis

It is thought that within the nucleolus, there are subcompartments for vectorial maturation of pre-ribosomes, with the transcription of the rDNA occurring at the interface between the FCs, where nascent transcripts reach out into the body of the DFC into the GC, as pre-rRNA processing occurs [reviewed in (45)]. With downregulation of NOP132, DDX47 appeared to be localized to the GC, but not to either the FC or DFC, suggesting that DDX47 is localized at the nucleolar periphery (probably the GC region) in the absence of NOP132 and that DDX47 might be retained in the FC

or DFC in the nucleolus by NOP132 during ribosome biogenesis. Consistently, FLAG-tagged DDX47 associated with 30S and 32S pre-rRNAs in the cell, indicating that DDX47 has a role in primary pre-rRNA processing.

It has been reported that NOP132/NOL8 is upregulated in diffuse-type gastric cancer and that downregulation of NOP132 induces apoptosis (19), suggesting that NOP132 is involved in carcinogenesis. We found that p53 co-precipitated with FLAG-NOP132. Although the association of NOP132 with p53 is suggestive, it is possible that over-expression of NOP132 is a consequence rather than an effector of carcinogenesis.

It was also reported that NOP132/NOL8 is a phosphoprotein (19). Consistently, NOP132 associated with several kinases that are involved in signal transduction (Table 1). Thus, these kinases might phosphorylate NOP132 and influence its function. It is also possible that NOP132 regulates DDX47 helicase activity either positively or negatively by associating with these kinases. Such is the case for telomere repeat binding factor (TRF) proteins and Bloom syndrome (BLM) helicase; the interaction of TRF1 and TRF2 with BLM has been reported to stimulate the BLM helicase activity (46,47).

The structure of the DEAD-box RNA helicases indicates that the HELICc domain is located downstream of the helicase domain (DEADc). In the HELICc domain, there are three conserved DEAD-box RNA helicase motifs, IV, V, and VI, within the HELICc domain (Figure 6c), that possibly function in substrate and γ phosphate binding (48). The region containing the HELICc motif of DDX47 interacted directly with the coiled-coil motif of NOP132 and was responsible for the nucleolar localization of the DDX47-EGFP fusion protein (Figure 6). Because DDX18 has a high level of amino acid identity with DDX47, especially in the HELICc motif, it is possible that both proteins interact with NOP132 through this motif. Although another DEAD-box RNA helicase, DDX21, was also found in the NOP132 complex (Figure 1a), direct interaction between DDX21 and NOP132 was not detected by yeast two-hybrid analysis (data not shown), suggesting that DDX21 binds to the NOP132 complex through interactions with other proteins or RNAs.

We previously reported that NOP132 could be the human counterpart of yeast Nop8 (15). Because Nop8-depleted cells contain reduced levels of free 60S ribosomes and polysomes and accumulate half-mer polysomes, Nop8 is probably involved in 60S ribosome biogenesis (16). Recently, it was reported that yeast Nop8 functionally interacts with DEAD-box RNA helicase Dbp6, which also interacts with Rpl3 and Rsa3, as shown by synthetic lethal mutant screening, and is involved in 60S ribosomal subunit formation (49). Dbp6 interacts with another DEAD-box RNA helicase, Dbp9, which is also involved in 60S ribosome biogenesis (50). A region of high similarity in amino acid sequences between NOP132 and Nop8 encompasses the DDX47-interacting region of NOP132, suggesting functional conservation between the two proteins and the involvement of NOP132 in 60S ribosome biogenesis. With regard to this possibility, we demonstrated that NOP132 associates with a novel nucleolar protein, NOP254/NNP72 (35), which is a human ortholog of yeast Npa1, which is a component of very early pre-60S ribosomal particles. Consistently, Npa1 is shown to associates with Nop8 and other nucleolar proteins (31,51). Together these data suggest that NOP132 participates in various stages of human ribosome biogenesis.

SUPPLEMENTARY DATA

Supplementary Data are available at NAR Online.

ACKNOWLEDGEMENTS

We thank Drs H. Kobayashi, H. Nishitani, K. Mihara, and N. Ishihara for helpful discussion and support. This work was supported by a Grant-in-Aid for Scientific Research on Priority Areas (T.S.), Grants-in-Aid for Specially Promoted Research (T.N.), and a Pioneer Research on Genome the Frontier, Ministry of Education, Culture, Sports, Science and Technology of Japan and a Grant-in-Aid for Science Research, from the Japan Society for the Promotion of Science (N.T.). Funding to pay the Open Access publication charges for this article was provided by Kyushu University.

Conflict of interest statement. None declared.

REFERENCES

1. Granneman,S. and Baserga,S.J. (2004) Ribosome biogenesis: of knobs and RNA processing. *Exp. Cell Res.*, **296**, 43–50.
2. Fromont-Racine,M., Senger,B., Saveanu,C. and Fasiolo,F. (2003) Ribosome assembly in eukaryotes. *Gene*, **313**, 17–42.
3. Venema,J. and Tollervey,D. (1999) Ribosome synthesis in *Saccharomyces cerevisiae*. *Annu. Rev. Genet.*, **33**, 261–311.
4. Takahashi,N., Yanagida,M., Fujiyama,S., Hayano,T. and Isobe,T. (2003) Proteomic snapshot analyses of preribosomal ribonucleoprotein complexes formed at various stages of ribosome biogenesis in yeast and mammalian cells. *Mass Spectrom Rev.*, **22**, 287–317.
5. Nishimoto,T. (2000) Upstream and downstream of ran GTPase. *Biol. Chem.*, **381**, 397–405.
6. Sazer,S. and Dasso,M. (2000) The ran decathlon: multiple roles of Ran. *J. Cell Sci.*, **113**, 1111–1118.
7. Shiomi,T., Fukushima,K., Suzuki,N., Nakashima,N., Noguchi,E. and Nishimoto,T. (1998) Human dis3p, which binds to either GTP- or GDP-Ran, complements *Saccharomyces cerevisiae* dis3. *J. Biochem. (Tokyo)*, **123**, 883–890.
8. Noguchi,E., Hayashi,N., Azuma,Y., Seki,T., Nakamura,M., Nakashima,N., Yanagida,M., He,X., Mueller,U., Sazer,S. *et al.* (1996) Dis3, implicated in mitotic control, binds directly to Ran and enhances the GEF activity of RCC1. *EMBO J.*, **15**, 5595–5605.
9. Suzuki,N., Noguchi,E., Nakashima,N., Oki,M., Ohba,T., Tartakoff,A., Ohishi,M. and Nishimoto,T. (2001) The *Saccharomyces cerevisiae* small GTPase, Gsp1p/Ran, is involved in 3′ processing of 7S-to-5.8S rRNA and in degradation of the excised 5′-A0 fragment of 35S pre-rRNA, both of which are carried out by the exosome. *Genetics*, **158**, 613–625.
10. Nakashima,N., Hayashi,N., Noguchi,E. and Nishimoto,T. (1996) Putative GTPase Gtr1p genetically interacts with the RanGTPase cycle in *Saccharomyces cerevisiae*. *J. Cell Sci.*, **109**, 2311–2318.
11. Nakashima,N., Noguchi,E. and Nishimoto,T. (1999) *Saccharomyces cerevisiae* putative G protein, Gtr1p, which forms complexes with itself and a novel protein designated as Gtr2p, negatively regulates the Ran/Gsp1p G protein cycle through Gtr2p. *Genetics*, **152**, 853–867.
12. Huang,J., Zhu,H., Haggarty,S.J., Spring,D.R., Hwang,H., Jin,F., Snyder,M. and Schreiber,S.L. (2004) Finding new components of the target of rapamycin (TOR) signaling network through chemical genetics and proteome chips. *Proc. Natl Acad. Sci. USA*, **101**, 16594–16599.

13. Dubouloz,F., Deloche,O., Wanke,V., Cameroni,E. and De Virgilio,C. (2005) The TOR and EGO protein complexes orchestrate microautophagy in yeast. *Mol. Cell*, **19**, 15–26.
14. Todaka,Y., Wang,Y., Tashiro,K., Nakashima,N., Nishimoto,T. and Sekiguchi,T. (2005) Association of the GTP-binding protein Gtr1p with Rpc19p, a shared subunit of RNA polymerase I and III in yeast *Saccharomyces cerevisiae*. *Genetics*, **170**, 1515–1524.
15. Sekiguchi,T., Todaka,Y., Wang,Y., Hirose,E., Nakashima,N. and Nishimoto,T. (2004) A novel human nucleolar protein, Nop132, binds to the G proteins, RRAG A/C/D. *J. Biol. Chem.*, **279**, 8343–8350.
16. Zanchin,N.I. and Goldfarb,D.S. (1999) Nip7p interacts with Nop8p, an essential nucleolar protein required for 60S ribosome biogenesis, and the exosome subunit Rrp43p. *Mol. Cell Biol.*, **19**, 1518–1525.
17. Zanchin,N.I., Roberts,P., DeSilva,A., Sherman,F. and Goldfarb,D.S. (1997) *Saccharomyces cerevisiae* Nip7p is required for efficient 60S ribosome subunit biogenesis. *Mol. Cell Biol.*, **17**, 5001–5015.
18. Hirose,E., Nakashima,N., Sekiguchi,T. and Nishimoto,T. (1998) RagA is a functional homologue of *S. cerevisiae* Gtr1p involved in the Ran/Gsp1-GTPase pathway. *J. Cell Sci.*, **111**, 11–21.
19. Jinawath,N., Furukawa,Y. and Nakamura,Y. (2004) Identification of NOL8, a nucleolar protein containing an RNA recognition motif (RRM), which was overexpressed in diffuse-type gastric cancer. *Cancer Sci.*, **95**, 430–435.
20. de la Cruz,J., Kressler,D. and Linder,P. (1999) Unwinding RNA in *Saccharomyces cerevisiae*: DEAD-box proteins and related families. *Trends Biochem. Sci.*, **24**, 192–198.
21. Abdelhaleem,M., Maltais,L. and Wain,H. (2003) The human DDX and DHX gene families of putative RNA helicases. *Genomics*, **81**, 618–622.
22. Sekiguchi,T., Hirose,E., Nakashima,N., Ii,M. and Nishimoto,T. (2001) Novel G proteins, Rag C and Rag D, interact with GTP-binding proteins, Rag A and Rag B. *J. Biol. Chem.*, **276**, 7246–7257.
23. Yanagida,M., Shimamoto,A., Nishikawa,K., Furuichi,Y., Isobe,T. and Takahashi,N. (2001) Isolation and proteomic characterization of the major proteins of the nucleolin-binding ribonucleoprotein complexes. *Proteomics*, **1**, 1390–1404.
24. Natsume,T., Yamauchi,Y., Nakayama,H., Shinkawa,T., Yanagida,M., Takahashi,N. and Isobe,T. (2002) A direct nanoflow liquid chromatography-tandem mass spectrometry system for interaction proteomics. *Anal. Chem.*, **74**, 4725–4733.
25. Sekiguchi,T., Nishimoto,T. and Hunter,T. (1999) Overexpression of D-type cyclins, E2F-1, SV40 large T antigen and HPV16 E7 rescue cell cycle arrest of tsBN462 cells caused by the CCG1/TAF(II)250 mutation. *Oncogene*, **18**, 1797–1806.
26. Chien,C.T., Bartel,P.L., Sternglanz,R. and Fields,S. (1991) The two-hybrid system: a method to identify and clone genes for proteins that interact with a protein of interest. *Proc. Natl Acad. Sci. USA*, **88**, 9578–9582.
27. Elbashir,S.M., Harborth,J., Lendeckel,W., Yalcin,A., Weber,K. and Tuschl,T. (2001) Duplexes of 21-nucleotide RNAs mediate RNA interference in cultured mammalian cells. *Nature*, **411**, 494–498.
28. Nishitani,H., Sugimoto,N., Roukos,V., Nakanishi,Y., Saijo,M., Obuse,C., Tsurimoto,T., Nakayama,K.I., Nakayama,K., Fujita,M. *et al.* (2006) Two E3 ubiquitin ligases, SCF-Skp2 and DDB1-Cul4, target human Cdt1 for proteolysis. *EMBO J.*, **25**, 1126–1136.
29. Sekiguchi,T., Miyata,T. and Nishimoto,T. (1988) Molecular cloning of the cDNA of human X chromosomal gene (CCG1) which complements the temperature-sensitive G1 mutants, tsBN462 and ts13, of the BHK cell line. *EMBO J.*, **7**, 1683–1687.
30. Hayano,T., Yanagida,M., Yamauchi,Y., Shinkawa,T., Isobe,T. and Takahashi,N. (2003) Proteomic analysis of human Nop56p-associated pre-ribosomal ribonucleoprotein complexes. Possible link between Nop56p and the nucleolar protein treacle responsible for Treacher Collins syndrome. *J. Biol. Chem.*, **278**, 34309–34319.
31. Dez,C., Froment,C., Noaillac-Depeyre,J., Monsarrat,B., Caizergues-Ferrer,M. and Henry,Y. (2004) Npa1p, a component of very early pre-60S ribosomal particles, associates with a subset of small nucleolar RNPs required for peptidyl transferase center modification. *Mol. Cell Biol.*, **24**, 6324–6337.
32. Yanagida,M., Hayano,T., Yamauchi,Y., Shinkawa,T., Natsume,T., Isobe,T. and Takahashi,N. (2004) Human fibrillarin forms a sub-complex with splicing factor 2-associated p32, protein arginine methyltransferases, and tubulins alpha 3 and beta 1 that is independent of its association with preribosomal ribonucleoprotein complexes. *J. Biol. Chem.*, **279**, 1607–1614.
33. Nachury,M.V., Ryder,U.W., Lamond,A.I. and Weis,K. (1998) Cloning and characterization of hSRP1 gamma, a tissue-specific nuclear transport factor. *Proc. Natl Acad. Sci. USA*, **95**, 582–587.
34. Doorbar,J., Elston,R.C., Napthine,S., Raj,K., Medcalf,E., Jackson,D., Coleman,N., Griffin,H.M., Masterson,P., Stacey,S. *et al.* (2000) The E1E4 protein of human papillomavirus type 16 associates with a putative RNA helicase through sequences in its C terminus. *J. Virol.*, **74**, 10081–10095.
35. Andersen,J.S., Lyon,C.E., Fox,A.H., Leung,A.K., Lam,Y.W., Steen,H., Mann,M. and Lamond,A.I. (2002) Directed proteomic analysis of the human nucleolus. *Curr. Biol.*, **12**, 1–11.
36. Warner,J.R. (1999) The economics of ribosome biosynthesis in yeast. *Trends Biochem. Sci.*, **24**, 437–440.
37. Andersen,J.S., Lam,Y.W., Leung,A.K., Ong,S.E., Lyon,C.E., Lamond,A.I. and Mann,M. (2005) Nucleolar proteome dynamics. *Nature*, **433**, 77–83.
38. Marchler-Bauer,A., Anderson,J.B., Cherukuri,P.F., DeWeese-Scott,C., Geer,L.Y., Gwadz,M., He,S., Hurwitz,D.I., Jackson,J.D., Ke,Z. *et al.* (2005) CDD: a Conserved Domain Database for protein classification. *Nucleic Acids Res.*, **33**, D192–196.
39. Burkhard,P., Stetefeld,J. and Strelkov,S.V. (2001) Coiled coils: a highly versatile protein folding motif. *Trends Cell Biol.*, **11**, 82–88.
40. O'Day,C.L., Chavanikamannil,F. and Abelson,J. (1996) 18S rRNA processing requires the RNA helicase-like protein Rrp3. *Nucleic Acids Res.*, **24**, 3201–3207.
41. Fatica,A., Cronshaw,A.D., Dlakic,M. and Tollervey,D. (2002) Ssf1p prevents premature processing of an early pre-60S ribosomal particle. *Mol. Cell*, **9**, 341–351.
42. Emery,B., de la Cruz,J., Rocak,S., Deloche,O. and Linder,P. (2004) Has1p, a member of the DEAD-box family, is required for 40S ribosomal subunit biogenesis in *Saccharomyces cerevisiae*. *Mol. Microbiol.*, **52**, 141–158.
43. Grandori,C., Mac,J., Siebelt,F., Ayer,D.E. and Eisenman,R.N. (1996) Myc-Max heterodimers activate a DEAD box gene and interact with multiple E box-related sites *in vivo*. *EMBO J.*, **15**, 4344–4357.
44. Winzeler,E.A., Shoemaker,D.D., Astromoff,A., Liang,H., Anderson,K., Andre,B., Bangham,R., Benito,R., Boeke,J.D., Bussey,H. *et al.* (1999) Functional characterization of the *S. cerevisiae* genome by gene deletion and parallel analysis. *Science*, **285**, 901–906.
45. Thiry,M. and Lafontaine,D.L. (2005) Birth of a nucleolus: the evolution of nucleolar compartments. *Trends Cell Biol.*, **15**, 194–199.
46. Opresko,P.L., von Kobbe,C., Laine,J.P., Harrigan,J., Hickson,I.D. and Bohr,V.A. (2002) Telomere-binding protein TRF2 binds to and stimulates the Werner and Bloom syndrome helicases. *J. Biol. Chem.*, **277**, 41110–41119.
47. Lillard-Wetherell,K., Machwe,A., Langland,G.T., Combs,K.A., Behbehani,G.K., Schonberg,S.A., German,J., Turchi,J.J., Orren,D.K. and Groden,J. (2004) Association and regulation of the BLM helicase by the telomere proteins TRF1 and TRF2. *Hum. Mol. Genet.*, **13**, 1919–1932.
48. Tanner,N.K. and Linder,P. (2001) DExD/H box RNA helicases: from generic motors to specific dissociation functions. *Mol. Cell*, **8**, 251–262.
49. de la Cruz,J., Lacombe,T., Deloche,O., Linder,P. and Kressler,D. (2004) The putative RNA helicase Dbp6p functionally interacts with Rpl3p, Nop8p and the novel trans-acting Factor Rsa3p during biogenesis of 60S ribosomal subunits in *Saccharomyces cerevisiae*. *Genetics*, **166**, 1687–1699.
50. Daugeron,M.C., Kressler,D. and Linder,P. (2001) Dbp9p, a putative ATP-dependent RNA helicase involved in 60S-ribosomal-subunit biogenesis, functionally interacts with Dbp6p. *RNA*, **7**, 1317–1334.
51. Rosado,I.V. and de la Cruz,J. (2004) Npa1p is an essential trans-acting factor required for an early step in the assembly of 60S ribosomal subunits in *Saccharomyces cerevisiae*. *RNA*, **10**, 1073–1083.